HHS Public Access

Author manuscript

Hum Mutat. Author manuscript; available in PMC 2023 December 01.

Published in final edited form as:

Hum Mutat. 2022 December ; 43(12): 1945–1955. doi:10.1002/humu.24452.

A loss-of-function cysteine mutant in fibulin-3 (EFEMP1) forms aberrant extracellular disulfide-linked homodimers and alters extracellular matrix composition

DaNae R. Woodard[1], **Steffi Daniel**[1], **Emi Nakahara**[1], **Ali Abbas**[1], **Sophia M. DiCesare**[1], **Gracen E. Collier**[1], **John D. Hulleman**[1,2]

[1]Department of Ophthalmology, University of, Texas Southwestern Medical Center, Dallas, Texas, USA

[2]Department of Pharmacology, University of, Texas Southwestern Medical Center, Dallas, Texas, USA

Abstract

Fibulin-3 (F3 or EFEMP1) is a disulfide-rich, secreted glycoprotein necessary for maintaining extracellular matrix (ECM) and connective tissue integrity. Three studies have identified distinct autosomal recessive *F3* mutations in individuals with Marfan Syndrome-like phenotypes. Herein, we characterize how one of these mutations, c.163T>C; p.Cys55Arg (C55R), disrupts F3 secretion, quaternary structure, and function by forming unique extracellular disulfide-linked homodimers. Dual cysteine mutants suggest that the C55R-induced disulfide species forms because of the new availability of Cys70 on adjacent F3 monomers. Surprisingly, mutation of single cysteines located near Cys55 (i.e., Cys29, Cys42, Cys48, Cys61, Cys70, Cys159, and Cys171) also produced similar extracellular disulfide-linked dimers, suggesting that this is not a phenomenon isolated to the C55R mutant. To assess C55R functionality, F3 knockout (KO) retinal pigmented epithelial (RPE) cells were generated, followed by reintroduction of wild-type (WT) or C55R F3. F3 KO cells produced lower levels of the ECM remodeling enzyme, matrix metalloproteinase 2, and reduced formation of collagen VI ECM filaments, both of which were partially rescued by WT F3 overexpression. However, C55R F3 was unable to compensate for these same ECM-related defects. Our results highlight the unique behavior of particular cysteine mutations in F3 and uncover potential routes to restore C55R F3 loss-of-function.

Keywords

disulfide bond; EFEMP1; extracellular matrix; fibulin-3; marfanoid syndrome

Correspondence: John D. Hulleman, Department of Ophthalmology, University of Texas Southwestern Medical Center, 5323, Harry Hines Blvd, Dallas, TX, USA. John.Hulleman@UTSouthwestern.edu.

SUPPORTING INFORMATION

Additional supporting information can be found online in the Supporting Information section at the end of this article.

CONFLICT OF INTEREST

The authors declare no conflict of interest.

1 | INTRODUCTION

Fibulin-3 (F3, encoded by the *EFEMP1* gene) is a secreted, disulfide-rich, extracellular matrix (ECM) glycoprotein of unclear function that is broadly expressed throughout the body (Daniel et al., 2020; Zhang & Marmorstein, 2010). Increasing evidence suggests the involvement of F3 in a variety of diseases ranging from gliomas (Hu et al., 2011), to marfanoid syndrome/connective tissue disorders (Bizzari et al., 2020; Driver et al., 2020; Verlee et al., 2021), to primary open angle glaucoma (Mackay et al., 2015), to age-related macular degeneration (Meyer et al., 2011), macular dystrophies (Hulleman, 2016; Stone et al., 1999), and general retinal dysfunction (Woodard, Nakahara, et al., 2021). Yet, knowledge of the factors that influence F3 protein homeostasis is limited. Specifically, how many disease-associated mutations alter F3 folding, secretion, and degradation is largely unknown. Moreover, how these mutations influence F3 behavior will lead to a better understanding of disease mechanisms and potentially rational therapies.

F3 is composed of six epidermal growth factor (EGF) domains, one of which is an atypical EGF domain containing an ~88 residue insert (Timpl et al., 2003; Zhang & Marmorstein, 2010), with the remaining five domains resembling canonical calcium-binding EGF (cbEGF) domains (Figure 1a). Structurally, each of these domains contain three disulfide bonds that form in a predictable pattern with numbering referring to the relative position of the cysteines within each domain: 1–3 (the “a” disulfide bond), 2–4 (the “b” disulfide bond), 5–6 (the “c” disulfide bond). F3 contains 40 cysteines, at least 30 of which are engaged in disulfide bonds. Previously, we demonstrated that mutation of cysteine residues in select canonical cbEGF domains results in protein nonsecretion and retention of F3 intracellularly (Hulleman et al., 2011; Woodard, Nakahara, et al., 2021), highlighting the importance of these residues in regulating F3 protein homeostasis. Recently, whole exome sequencing of a pair of siblings with marfanoid syndrome revealed a new homozygous cysteine missense mutation (c.163T>C; p.Cys55Arg, C55R) in F3 (Bizzari et al., 2020). Patients with this homozygous mutation presented with tall stature, inguinal hernias, and advanced bone age, among other features (Bizzari et al., 2020). Due to its mode of inheritance, and because additional studies identified biallelic loss-of-function mutations in *EFEMP1* in unrelated individuals also with Marfan-like connective tissue disorders (Driver et al., 2020; Verlee et al., 2021), this C55R mutation likely renders F3 functionally inactive. Yet, how this mutation disrupts the F3 function is unknown. The C55 residue is located in the atypical EGF domain 1 (D1) which is not annotated in Uniprot to have disulfide bonds, most likely due to a lack of experimental evidence to support these assignments. None-theless, regardless of the in silico annotation, it is quite likely that the C55 residue is involved in disulfide bond formation within the atypical EGF domain and is important for F3 structural regulation. Herein, we experimentally determined how the C55R mutation alters F3 secretion, intracellular levels, and quaternary structure when produced in cultured cells. Moreover, we demonstrate that C55R F3 is unable to compensate for ECM changes driven by loss of endogenous F3, confirming that this mutation is indeed loss-of-function.

2 | MATERIALS AND METHODS

2.1 | Plasmid generation

Cysteine mutations were introduced into a pENTR1A FLAG (FT) WT F3 or pENTR1A 3xFT WT F3 plasmid using the Q5 Site-Directed Mutagenesis Kit (New England Biolabs). pENTR1A constructs were shuttled into the pcDNA DEST40 vector (Life Technologies) or the pLenti CMV Puro DEST vector (a gift from Eric Campeau and Paul Kaufman, Addgene plasmid #17452) by an LR clonase II reaction (Life Technologies) to generate the final construct used for transfection/infection. pcDNA 3xFT HiBiT F3 constructs incorporated three FLAG sequences (DYKDHDGDYKDHDIDYKDDDDK) followed by a GGVSGYRLFKKIS peptide (HiBiT sequence underlined) and the remainder of F3. All FLAG-containing constructs contain the FLAG sequence immediately after the signal sequence. All F3 mutations and plasmids were verified by Sanger sequencing.

2.2 | Cell culture and transfection

Human embryonic kidney cells (HEK-293A; Life Technologies CA or AAVpro-293T; Takara) were cultured at 37°C with 5% CO_2 in Dulbecco's minimal essential medium (DMEM) supplemented with high glucose, (4.5 g/L; Corning), 10% fetal bovine serum (FBS; Omega Scientific), and 1% penicillin-streptomycin-glutamine (PSQ; Gibco). Normal dermal fibroblasts (PCS-201-012; ATCC) were cultured similarly but in DMEM media containing low glucose. ARPE-19 cells (CRL-2302; ATCC) were cultured in DMEM/F12 media supplemented with 10% FBS and PSQ. Cells were plated at a density of ~100,000 cells/well in a 24-well plate and transfected the following day with 500 ng of midi-prepped endotoxin-free plasmid DNA (Qiagen) using Lipofectamine 3000 (Life Technologies) as described previously (Woodard, Nakahara, et al., 2021; Woodard, Xing, et al., 2021). Forty-eight hours after transfection, fresh serum-free media was added. Cells were harvested and media was collected 24 h later (72 h posttransfection). For cotransfection experiments, cells were plated overnight at a density of 120,000 cells/well of a 12-well plate. 500 ng of each plasmid was used combined with 1 μl of P3000 and 3 μl Lipofectamine 3000 in OptiMEM. The next day, fresh media containing 0.5% FBS was added. Media was assayed 24 h later by HiBiT blotting and standard western blot analysis (48 h postinitial transfection). To generate stably expressing F3 cell lines, HEK-293A, ARPE-19, AAVpro-293T, or dermal fibroblasts cells were infected with VSV-G-pseudotyped lentivirus packaged (described in more detail previously [Ramadurgum & Hulleman, 2020; Ramadurgum et al., 2020]) with the pLenti CMV Puro vector containing 3xFT WT, 3xFT C55R F3, or 3xFT C171A F3. Stable populations were selected using puromycin (1 μg/ml).

2.3 | Western and HiBiT blotting

For western blot analysis, cells were washed with Hanks buffered salt solution (HBSS; Sigma-Aldrich), then lysed with radioimmunoprecipitation assay (RIPA) buffer (Santa Cruz) supplemented with Halt protease inhibitor (Pierce) and benzonase (Millipore Sigma) for 3–5 min at RT and spun at max speed (14,800 rpm) at 4°C for 10 min. The soluble supernatant was collected and protein concentration was quantified via bicinchoninic assay (Pierce Thermo Scientific). Normalized soluble supernatant or 20 μl of conditioned media was run on a 4%–20% Tris-Gly SDS-PAGE gel (Life Technologies) and transferred onto

a nitrocellulose membrane using an iBlot2 device (P0 program; Life Technologies). After probing for the total transferred protein using Ponceau S (Sigma-Aldrich), membranes were blocked overnight in Odyssey Blocking Buffer (LICOR). Membranes were probed with rabbit anti-FLAG (1:5000; Thermo Fisher Scientific, cat # PA1-984B), mouse anti-FLAG M2 (1:1000; Sigma-Aldrich, cat# F1804), rabbit antiF3 (1:500; ProSci; Poway; CA, cat# 5213), or mouse anti-β-actin (1:1000; Sigma-Aldrich; cat# A1978) for 1 h at RT followed by washes with TBS-T and an appropriate NIR-conjugated secondary antibody (LI-COR). All Western blot imaging was performed on an Odyssey CLx (LI-COR). A similar process was used for Nano-Glo HiBiT blotting (Promega) wherein samples were prepared for SDS-PAGE, transferred to nitrocellulose membranes and then incubated in TBS-T for 30 min at RT. Blots were then incubated in 1x HiBiT blotting buffer supplemented with LgBiT (1:200) and Nano-Glo substrate (1:100) for 5 min at RT. Chemiluminescence was imaged using a LI-COR Fc. Images and band quantification were performed using Image Studio software (LI-COR).

2.4 | Immunoprecipitation (IP) and mass spectrometry

Serum-free media was collected from Hyperflasks (Corning) containing HEK-293A cells stably-expressing 3xFT C55R F3 or AAVpro-293T cells stably expressing 3xFT C171A F3 and transferred to 50 ml conical tubes. A small aliquot (~20–25 μl) of anti-FLAG M2 magnetic beads (Millipore Sigma) was added to each tube and allowed to rotate overnight at 4°C. The following day, tubes were spun at 500 rpm for 1–3 min. A large magnetic rack was used to capture the beads and the media was aspirated. The beads were washed three times with cold HBSS buffer followed by transfer to a 1.5 ml tube after the last wash. Samples were eluted with 100–200 μg/ml of 3xFLAG peptide (Millipore Sigma, cat #F4799) in TBS, rotated for ≥30 min and the supernatant was collected by placing samples in a small magnetic rack. Samples were then run on a 4%–20% Tris-Gly SDS-PAGE gel (Life Technologies) followed by Coomassie Blue staining. Bands from immunoprecipitated samples were visualized using an Amersham Imager 600 (GE Healthcare), and the protein band at ~110 kDa for C55R F3 or ~130 kDa for C171A F3 was manually excised, placed in a 1.5 ml Eppendorf tube, and submitted to the UT Southwestern Proteomics Core for analysis.

2.5 | F3 knockout (KO) cell generation

F3 KO cells were generated through a failed attempt to perform homology directed repair to generate point mutations in the F3 gene. Briefly, low passage ARPE-19 cells were electroporated (1400 V, 20 ms, two pulses, Neon Transfection System; Life Technologies) with a CRISPR/Cas9 ribonucleoprotein containing Alt-R tracrRNA/crRNA duplex (gRNA: GACCACAAATGAATGCCGGG), Alt-R HiFi S.p. Cas9 nuclease V3, and a single stranded oligonucleotide (all from Integrated DNA Technologies). After electroporation, cells were expanded and submitted for cell sorting (UT Southwestern Flow Cytometry Core). Single colony clones were isolated, grown, and their mRNA was extracted (Aurum Total RNA Mini kit; BioRad) and analyzed for F3 expression (described previously [Woodard, Nakahara, et al., 2021]), identifying KO cells in the process. These cells were then used as parental cells to generate the 3xFT WT F3 and 3xFT C55R F3 overexpression lines. Genomic validation of F3 editing was accomplished by extraction of

genomic DNA (GenElute; Sigma) followed by amplification of F3 exon 9 (forward primer: 5′AATTAGATCAGTTCATTAGTTTAGTTAGTAAACTCTTTGACCCT-3′; reverse primer: 5′-TGCAGAGACAAACAAAAGTATTCAGCAGTTTG3′) and insertion into the pCR-4 vector using TOPO-TA cloning (Thermo Fisher Scientific), colony isolation and Sanger sequencing using the T3 forward primer (5′-GCAATTAACCCTCACTAAAGG-3′).

2.6 | Zymography

ARPE-19 cells were plated overnight at a density of 100,000 cells/well of a 12-well polyester transwell (0.4 μm pore size, 1.12 cm^2 surface area; Corning) in full serum-containing media. The next day, the media was changed to serum-free media, and was changed every 3–4 days thereafter for 2 weeks. Before initiating zymography, cells were incubated in serum-free media for 72 h. Apical and basal aliquots were taken, mixed with nonreducing SDS-PAGE buffer, and loaded onto a 10% gelatin gel (9–10 μl for apical, 18–20 μl for basal, Novex; Life Technologies). Samples were electrophoresed for ~90 min at 125–140 V. The gel was then incubated in renaturing buffer (30 min at RT; Novex), followed by incubation in developing buffer (30 min at RT; G-Biosciences), and again in fresh developing buffer overnight at 37°C with gentle shaking. Gels were stained with Coomassie R-250 for 1 h at RT, followed by destaining to reveal digested gelatin corresponding to matrix metalloproteineases (MMP2) activity. Gels were imaged on an Odyssey CLx (LI-COR) using the 700 nm channel and quantified using Image Studio (LI-COR).

2.7 | ECM analysis

Cells were seeded in transwells and treated as described above in the zymography section. After 2 weeks, the transwells were washed 3x with Dulbecco's phosphate-buffered saline (Gibco) and decellularized by incubation with 0.5% Triton-X 100 and 20 mM ammonium hydroxide for 5 min at 37°C with gentle shaking (Fernandez-Godino et al., 2018). Samples were washed 1x in DPBS followed by fixation in 4% PFA for 30 min at RT. Transwells were then washed 2x in DPBS and blocked for 1 h at RT in 10% goat serum, 0.1% BSA, 0.1% Triton-X dissolved in PBS. The primary antibody (rabbit antiColVI, 1:200; Abcam #ab6588) was incubated at 4°C overnight with gentle rocking. Membranes were washed 2x followed by secondary antibody (anti-rabbit AlexaFluor 488 or 594, 1:1000; Life Technologies), for 2 h at RT. After two additional DPBS washes, DAPI was added (to confirm decellularization), incubated for 5–10 min at RT and then transwells were washed again one final time before excision and mounted on glass slides with a drop of ProLong Diamond Antifade (Life Technologies). Images were acquired at either ×63 or ×25 magnification using a Leica TCS SP8 confocal microscope (Leica Microsystems) and analyzed using ImageJ (NIH). The images presented were acquired by z-scanning (~15 steps, 0.37 μm each) at ×63 magnification.

2.8 | Statistical analysis

To determine statistical significance, samples were compared using either a one-sample *t*-test using Excel against a hypothetical value of 1 (i.e., unchanged compared to the control), or a two-sample unpaired *t*-test. Significance was set at $*p < 0.05$, $**p < 0.01$, and $***p < 0.001$.

3 | RESULTS

3.1 | Secreted C55R F3 forms an extracellular disulfide-linked dimer

Bizzari et al. (2020) identified a homozygous C55R mutation in the atypical EGF domain (D1, Figure 1a) of F3 as the causative mutation resulting in marfanoid syndrome in two siblings. A priori, one might speculate that this mutation would cause protein nonsecretion and intracellular retention, similar to what we have observed previously with engineered cysteine to alanine mutations in cbEGF domain 6 (D6) of F3 (Supporting Information: Figure S1A,B) (Hulleman et al., 2011; Woodard, Nakahara, et al., 2021). Surprisingly, after transfection of FLAG-tagged (FT) C55R F3 in HEK-293A cells, we found that under reducing conditions, the C55R variant was secreted at similar levels to wild-type (WT) F3 (Figure 1b, upper left panel, 0.89 ± 0.12 vs. WT levels), and that intracellular C55R steady state levels were elevated (Figure 1b, left middle panel 1.59 ± 0.15 vs. WT levels), resulting in a significantly reduced secretion propensity (defined as secreted/intracellular relative to WT F3 values, 0.56 ± 0.04 relative to WT, $p < 0.001$, Figure 1c). Yet, under nonreducing conditions, we found that in addition to a monomeric form of F3 with a slightly slower migration pattern relative to WT F3, the C55R variant also forms a secreted disulfide linked dimer at ~110 kDa (Figure 1b, right upper panel, arrow). Under these same conditions, no detectable dimeric WT or C55R F3 was observed in the cell lysates (Figure 1b, right middle panel). Additional experiments using untagged C55R F3 in HEK-293A cells demonstrated that the media dimerization is not due to influence of the FLAG tag (Supporting Information: Figure S2A). However, due to its versatility and cleanliness of detection (e.g., see multiple nonspecific bands [*] in Supporting Information: Figure S2A), we continued to use FLAG-tagged F3 constructs for the remainder of this work. C55R extracellular dimerization was also clearly observed in the conditioned media of dermal fibroblasts overexpressing F3 (Supporting Information: Figure S2B). Moreover, alkylation of conditioned media with iodoacetamide before boiling in nonreducing sample buffer demonstrated that this disulfide species is not forming aberrantly during sample preparation (Supporting Information: Figure S3). Mass spectrometry analysis of the dimer band purified by FLAG immunoprecipitation revealed that F3 was by far the most abundant protein in the 110 kDa C55R band (1.04×10^8 spectral counts, Supporting Information: Table S1), and other identified proteins (between 40 and 90 kDa) were >10-fold lower in abundance than F3 (Supporting Information: Table S1). Overall, these data suggest that the C55R variant leads to a unique, dimerized quaternary structure primarily outside of the cell.

3.2 | The C55R mutant forms homodimers

Although we have shown that C55R forms extracellular disulphide-linked dimers, it was unclear whether these dimers consisted of only C55R (homodimers) or if they also recruited WT F3 (heterodimers), both of which would be detected as F3 in the mass spectrometry results. To address this point, we performed cotransfection experiments with WT F3 and C55R containing different epitope tags (FT or 3xFT HiBiT [Dixon et al., 2016]). 3xFT HiBiT WT F3 cotransfected with FT C55R F3 was not recruited to form any detectable dimer as determined by HiBiT blotting using nonreducing conditions (Figure 2a), indicating a lack of interaction between WT and C55R F3. However, 3xFT HiBiT C55R F3 (Figure 2a,c) and FT C55R F3 (Figure 2b) both formed dimeric species under the same conditions.

These results are consistent with the observation that individuals heterozygous for the C55R mutation appear to be unaffected (or at least not severely affected), seem to retain sufficient activity of WT F3 to prevent marfanoid symptoms (Bizzari et al., 2020), and that this mutation does not initiate disease through a dominant negative mechanism on WT F3.

3.3 | Mutation of additional N-terminal cysteines in F3 also renders it prone to extracellular disulfide-linked dimerization

We next asked the question of whether the disulfide-linked dimer caused by the C55R mutation was unique to mutation of this particular residue, or if it was a shared phenomenon common of other N-terminal cysteine mutants in F3. To answer this question, we generated a panel of alanine substitutions at each of the first eight cysteine residues (C29, C42, C48, C55, C61, C70, C159, and C171) spanning D1 and immediately before it (Figure 1a). Additionally, as controls, we included alanine mutations of the last two cysteines in F3 (C379, C386), which have not been assigned disulfide bonds (Uniprot, https://www.uniprot.org/uniprot/Q12805). Each of these cysteine mutations significantly decreased the secretion propensity of F3 to a greater degree than the C55R mutation (Figure 3a,b), suggesting that they are all important for F3 secretion and are likely engaged in transient disulfide linkages during F3 folding or in final native disulfide bonds in mature F3 (Chang et al., 1995, 2001). Similar to the C55R variant, mutation of the remaining first five cysteines in F3 (C29, C42, C48, C61, or C70) also caused disulfide linked dimers at ~110 kDa under nonreducing conditions, although they did so to varying degrees (Figure 3a, right upper panel, solid arrow), suggesting that formation of the dimer is not unique to only the C55R variant. Interestingly, C159A and C171A, which are located after the insertion region in D1 (Figure 1a), formed higher molecular weight species migrating closer to ~130 kDa (Figure 3a, right upper panel, dashed arrow), suggesting the presence of a distinct conformation compared to the first six cysteine mutants before the D1 insert region. We subsequently confirmed that this 130 kDa species was also dimeric F3 by performing mass spectrometry analysis of the apparent dimer band purified by FLAG immunoprecipitation (3.57×10^9 spectral counts, Supporting Information: Table S2). Other identified proteins (between 40 and 90 kDa) were >20-fold lower in abundance than F3 (Supporting Information: Table S2). Interestingly, only a small amount of secreted monomeric F3 was found for the C379A and C386A F3 variants (Figure 3a, right upper panel) located in the region immediately after D6 (Figure 1a). Importantly, as with the C55R variant, the observed dimeric species for these additional cysteine mutations were also not due to aberrant disulfide bonding during sample preparation (Supporting Information: Table S3). Overall, these observations suggest that quality control mechanisms regulating F3 disulfide bonding, folding and secretion appear to tolerate similar mutations vastly differently depending on their location within the F3 protein, a finding which is similar to what we have postulated when analyzing other engineered and clinically-identified mutations (Nguyen & Hulleman, 2015; Woodard, Nakahara, et al., 2021).

3.4 | Dual cysteine mutations in the atypical EGF domain clarify the residues responsible for disulfide dimer formation

We speculated that the dimerization observed with the single cysteine-to-alanine mutations (Figure 3a) in and surrounding D1 were due to new accessibility of the partner cysteine

which would normally have been engaged in disulfide bonding in native F3. Thus, we hypothesized that elimination of the mutated cysteine's disulfide bonding partner would eliminate the disulfide dimer and also shed light on the disulfide structure composition of D1. Since Uniprot defines the beginning of D1 as residue 26, disulfide bonding would be predicted to follow standard patterning for EGF domains (Arolas et al., 2006; Chang et al., 1995, 2001), and the bonding order would be C29[a_n]–C48[a_c] (wherein the subscript indicates which residue is located closer to the N- or C-terminus), C42[b_n]–C55[b_c], C61[c_n]–C70[c_c], followed by C159[‘d’$_n$]–C171[‘d’$_c$] (designated as such because it seems to be an extraneous disulfide bond under this numbering, Figure 4a). However, we hypothesized that the beginning of D1 is actually at residue 44, which is the start of exon 4 in *EFEMP1*, beginning with the canonical cbEGF leader sequence, Asp-Ile-Asp-Glu (DIDE). In fact, each of the cbEGF domains in F3 are located within their own exon (exons 5–9) and begin with the amino acids DIDE or Asp-Ile-Asn-Glu (DINE) in each instance (Benchling, https://benchling.com/, ENSG00000115380). Thus, we speculate that the actual disulfide pattern is C29[a’$_n$]-C42[a’$_c$] (designated as such because it occurs before the a_n and a_c disulfide bond), C48[a_n]–C61[a_c], C55[b_n]–C70[b_c] followed by C159[c_n]–C171[c_c] (Figure 4b). Based on this hypothesis, we predicted that in the C55R background, mutating C42 to an alanine (the supposed disulfide bonding partner according to Uniprot, Figure 4a) would not have any effect on C55R dimer formation. Indeed, this is what we observed (Figure 4c, arrow). However, mutation of C70 to alanine in the C55R background eliminated the ~110 kDa dimeric species (Figure 4c, arrow), supporting our proposed disulfide bonding pattern (Figure 4b). Further backing of our revised disulfide bonding pattern arises from the observation that the dual C29A/C42A mutant also eliminated the ~110 kDa species observed with the single C29A or C42A mutations (suggesting that these residues form a disulfide linkage), and that the C159A/C171A dual mutation substantially reduced the 130 kDa dimeric species typically observed in the single C159A and C171A mutants (Figure 4c). Interestingly, in many cases, there appears to be an interplay between the 110 and 130 kDa dimeric species. For example, reduction of the 130 kDa band leads to what seems to be a small increase in the 110 kDa dimeric band and vice versa. These observations highlight the complexity of disulfide bonding in EGF domains and within the F3 protein.

3.5 | F3 knockout cells demonstrate alterations in metalloproteinase activity and collagen VI assembly which are not rescuable by the C55R F3 variant

To develop a cellular background in which we could test whether C55R F3 is truly a loss-of-function mutation, we knocked out F3 in a RPE cell line by CRISPR/Cas9 gene editing (Supporting Information: Figure S4A,C). While the physiological function of F3 is not completely clear and is most likely tissue and context-dependent, previous studies have suggested that mutations in F3 can alter MMP2 and ECM formation (Fernandez-Godino, 2018; Fernandez-Godino et al., 2018). Moreover, we have found that F3 KO mice have defective corneas (Daniel et al., 2020), which are largely composed of type VI collagen (ColVI) (Doane et al., 1992; Zimmermann et al., 1986). Thus, we chose to measure the activity and ECM structure of these two proteins, MMP2 and ColVI, which have also been implicated in Marfan syndrome (Ikonomidis et al., 2006; Xiong et al., 2012) or myopathies (Allamand et al., 2011), in unedited ARPE-19 cells, F3 KO cells, and F3 KO cells with overexpressed 3xFT WT F3 or 3xFT C55R F3 (Supporting Information: Figure S4B). F3

KO cells demonstrated a significant reduction in MMP2 activity as determined by gelatin zymography, which was partially rescued by overexpressing 3xFT WT F3 in the F3 KO background (Figure 5a,b). However, overexpression of similar amounts of 3xFT C55R F3 did not rescue this MMP2 defect (Figure 5a,b). Similarly, F3 KO cells showed a clear defect in ColVI ECM filament formation, which again was partly restored by 3xFT WT F3 overexpression (Figure 5c). Expression of 3xFT C55R, on the other hand, was not able to rescue ColVI network formation (Figure 5c). It is interesting to speculate that the asthenic and thin appearance of homozygous C55R patients (Bizzari et al., 2020) (combined with their reduced muscle strength) could be due to F3-dependent ColVI-related muscle defects (Allamand et al., 2011). The combination of these results in RPE cells strongly suggest a C55R loss-of-function mechanism, yet additional experimentation is required to demonstrate this to a more definitive degree.

4 | DISCUSSION

We report the first known instance of F3 disulfide-induced dimerization triggered by the marfanoid-syndrome-associated C55R mutation. This aberrantly formed species is detected extracellularly and appears to be a result of a C70–C70 disulfide bond on adjacent monomers. Yet, this general disulfide dimerization phenomenon does not appear to be solely unique to the C55R mutation since additional engineered cysteine-to-alanine mutations in and surrounding the atypical EGF domain region also lead to variable levels of disulphide-linked extracellular dimer. Moreover, we have demonstrated that removal of F3 from ECM-producing cells (RPE cells in this case) results in significant changes to ECM remodeling enzymes (e.g., decreased MMP2) and the morphology of prominent ECM proteins (e.g., ColVI). While overexpression of WT F3 could partially compensate for these defects, similar levels of C55R F3 overexpression did not rescue these phenotypes, reaffirming that it is a loss-of-function mutation. Yet, the data that we present on this marfanoid-associated mutation likely encompasses only a portion of the broader story of how mutations in F3 influence connective tissue disorders. Previous mutations in F3 result in premature stop codons, and in some verified instances, results in nonsense-mediated mRNA decay (NMD [Driver et al., 2020]). Whether this is true for additional identified F3 nonsense mutations (Verlee et al., 2021) is currently unclear. Thus, it is possible that F3 mutations associated with connective tissue disorders influence disease by diverse mechanisms (i.e., lack of F3, truncated F3, misfolded F3, or dominant-negative F3). To help address these uncertainties, future studies should be directed to (i) assessing F3 transcript levels from patient-derived fibroblasts, (ii) defining the biochemical behavior of mutations that result in truncated F3, but do not lead to NMD, (iii) defining potential differences in F3 interacting partners (e.g., trpoelsatin, TIMP3, ECM1, etc.) among newly identified variants, (iv) understand the contributions of intracellularly retained F3 versus the contributions of secreted F3 with respect to ECM formation and general cell/tissue health, (v) understanding how the ECM changes when F3 is absent, and (vi) understand the importance/relevance of ER stress induced by select cysteine mutants of F3 (Supporting Information: Figure S5) to ECM synthesis and formation.

The observation that multiple additional cysteine mutations (C29, C42, C48, C16, C70, C159, and C171) in the atypical EGF domain region lead to similar extracellular disulfide-

linked dimers begs the question of whether additional cysteine mutations in F3 could also lead to a nonfunctional F3 and result in marfanoid phenotypes through similar molecular behaviors. While such mutations have not yet been identified and annotated in clinical variant databases (e.g., ClinVar, https://www.ncbi.nlm.nih.gov/clinvar/), it is quite possible that they exist in the human population, but commonly do not result in disease because of their autosomal recessive nature. Indeed, the C55R mutation would likely have not been identified if it were not for consanguinity (Bizzari et al., 2020). Our observations also raise an intriguing question of whether oxidation of certain reactive cysteine residues during normal physiology or oxidative stress could alter the structure and therefore function of F3 and the composition/dynamics of the ECM.

In our analysis of this new C55R variant, as well as all the other cysteine mutants located near the atypical EGF domain, we were surprised to not detect any intracellular F3 disulfide bonding. While we cannot rule out the idea of intracellular disulfide formation below our current level of detection, or intracellular disulfide formation followed by efficient secretion from the cell, extracellular disulfide bond formation appears to be a relatively unique phenomenon generally associated with coagulation (thrombus/fibrin generation) (Cho et al., 2008; Popescu et al., 2010). It will be interesting to more definitively test whether cysteine-mutated F3 could also be a substrate of extracellular protein disulfide isomerases.

Moving forward, our data also provide clues for potentially treating C55R-associated marfanoid syndrome. We speculate that elimination of the extracellular dimeric species may be able to restore some degree of F3 function within the ECM. To accomplish this, it could be possible to use selective, covalent cysteine nucleophiles to target and modify the two C70 residues on adjacent F3 monomers which seem to facilitate the ~110 kDa C55R dimer formation. Such an approach, which was previously thought to be too nonspecific to be useful, has gained recent momentum and promise for other proteins (Hallenbeck et al., 2017; Resnick et al., 2019). Whether this approach would be feasible and/or beneficial in treating C55R-related marfanoid syndrome remains to be determined.

Supplementary Material

Refer to Web version on PubMed Central for supplementary material.

ACKNOWLEDGMENTS

J. D. H. is supported by an endowment from the Roger and Dorothy Hirl Research Fund, and R01 EY027785. D. R. W. was supported by an NIH Diversity Supplement. A. A. was supported by an NIH T35 Training Grant (T35 EY026510). Additional support was provided by a National Eye Institute Visual Science Core Grant (P30 EY030413, to the UT Southwestern Department of Ophthalmology). Roger and Dorothy Hirl Research Fund, R01 EY027785, NIH Diversity Supplement (EY027785), T35 EY026510, P30 EY030413.

Funding information

Roger and Dorothy Hirl Research Fund; National Eye Institute

REFERENCES

Allamand V, Brinas L, Richard P, Stojkovic T, Quijano-Roy S, & Bonne G. (2011). ColVI myopathies: Where do we stand, where do we go? Skeletal Muscle, 1, 30. 10.1186/2044-5040-1-30 [PubMed: 21943391]

Arolas JL, Aviles FX, Chang JY, & Ventura S. (2006). Folding of small disulfide-rich proteins: Clarifying the puzzle. Trends in Biochemical Sciences, 31(5), 292–301. [PubMed: 16600598]

Bizzari S, El-Bazzal L, Nair P, Younan A, Stora S, Mehawej C, El-Hayek S, Delague V, & Mégarbané A. (2020). Recessive marfanoid syndrome with herniation associated with a homozygous mutation in Fibulin-3. European Journal of Medical Genetics, 63(5), 103869. 10.1016/j.ejmg.2020.103869

Chang JY, Li L, & Lai PH (2001). A major kinetic trap for the oxidative folding of human epidermal growth factor. Journal of Biological Chemistry, 276(7), 4845–4852. 10.1074/jbc.M005160200 [PubMed: 11087730]

Chang JY, Schindler P, Ramseier U, & Lai PH (1995). The disulfide folding pathway of human epidermal growth factor. Journal of Biological Chemistry, 270(16), 9207–9216. [PubMed: 7721838]

Cho J, Furie BC, Coughlin SR, & Furie B. (2008). A critical role for extracellular protein disulfide isomerase during thrombus formation in mice. Journal of Clinical Investigation, 118(3), 1123–1131. 10.1172/JCI34134 [PubMed: 18292814]

Daniel S, Renwick M, Chau VQ, Datta S, Maddineni P, Zode G, Wade EM, Robertson SP, Petroll WM, & Hulleman JD (2020). Fibulin-3 knockout mice demonstrate corneal dysfunction but maintain normal retinal integrity. Journal of Molecular Medicine (Berlin, Germany), 98(11), 1639–1656. 10.1007/s00109-020-01974-z [PubMed: 32964303]

Dixon AS, Schwinn MK, Hall MP, Zimmerman K, Otto P, Lubben TH, Butler BL, Binkowski BF, Machleidt T, Kirkland TA, Wood MG, Eggers CT, Encell LP, & Wood KV (2016). NanoLuc complementation reporter optimized for accurate measurement of protein interactions in cells. ACS Chemical Biology, 11(2), 400–408. 10.1021/acschembio.5b00753 [PubMed: 26569370]

Doane KJ, Yang G, & Birk DE (1992). Corneal cell-matrix interactions: Type VI collagen promotes adhesion and spreading of corneal fibroblasts. Experimental Cell Research, 200(2), 490–499. 10.1016/0014-4827(92)90200-r [PubMed: 1572410]

Driver S, Jackson MR, Richter K, Tomlinson P, Brockway B, Halliday BJ, Markie DM, Robertson SP, & Wade EM (2020). Biallelic variants in EFEMP1 in a man with a pronounced connective tissue phenotype. European Journal of Human Genetics, 28(4), 445–452. 10.1038/s41431-019-0546-7 [PubMed: 31792352]

Fernandez-Godino R. (2018). Alterations in extracellular Matrix/Bruch's membrane can cause the activation of the alternative complement pathway via tick-over. Advances in Experimental Medicine and Biology, 1074, 29–35. 10.1007/978-3-319-75402-4_4 [PubMed: 29721924]

Fernandez-Godino R, Bujakowska KM, & Pierce EA (2018). Changes in extracellular matrix cause RPE cells to make basal deposits and activate the alternative complement pathway. Human Molecular Genetics, 27(1), 147–159. 10.1093/hmg/ddx392 [PubMed: 29095988]

Hallenbeck KK, Turner DM, Renslo AR, & Arkin MR (2017). Targeting non-catalytic cysteine residues through structure-guided drug discovery. Current Topics in Medicinal Chemistry, 17(1), 4–15. 10.2174/1568026616666160719163839 [PubMed: 27449257]

Hu Y, Pioli PD, Siegel E, Zhang Q, Nelson J, Chaturbedi A, Mathews MS, Ro DI, Alkafeef S, Hsu N, Hamamura M, Yu L, Hess KR, Tromberg BJ, Linskey ME, & Zhou YH (2011).EFEMP1 suppresses malignant glioma growth and exerts its action within the tumor extracellular compartment. Molecular Cancer, 10, 123. 10.1186/1476-4598-10-123 [PubMed: 21955618]

Hulleman JD (2016). Malattia Leventinese/Doyne honeycomb retinal dystrophy: Similarities to age-related macular degeneration and potential therapies. Advances in Experimental Medicine and Biology, 854, 153–158. 10.1007/978-3-319-17121-0_21 [PubMed: 26427406]

Hulleman JD, Kaushal S, Balch WE, & Kelly JW (2011). Compromised mutant EFEMP1 secretion associated with macular dystrophy remedied by proteostasis network alteration. Molecular Biology of the Cell, 22(24), 4765–4775. 10.1091/mbc.E11-08-0695 [PubMed: 22031286]

Ikonomidis JS, Jones JA, Barbour JR, Stroud RE, Clark LL, Kaplan BS, Zeeshan A, Bavaria JE, Gorman JH, Spinale FG, & Gorman RC (2006). Expression of matrix metalloproteinases and

endogenous inhibitors within ascending aortic aneurysms of patients with Marfan syndrome. Circulation, 114(1 Suppl), I365–I370. 10.1161/CIRCULATIONAHA.105.000810 [PubMed: 16820601]

Mackay DS, Bennett TM, & Shiels A. (2015). Exome sequencing identifies a missense variant in EFEMP1 Co-segregating in a family with autosomal dominant primary open-angle glaucoma. PLoS One, 10(7), e0132529. 10.1371/journal.pone.0132529

Meyer KJ, Davis LK, Schindler EI, Beck JS, Rudd DS, Grundstad AJ, Scheetz TE, Braun TA, Fingert JH, Alward WL, Kwon YH, Folk JC, Russell SR, Wassink TH, Stone EM, & Sheffield VC (2011). Genome-wide analysis of copy number variants in age-related macular degeneration. Human Genetics, 129(1), 91–100. 10.1007/s00439-010-0904-6 [PubMed: 20981449]

Nguyen A, & Hulleman JD (2015). Differential tolerance of 'pseudopathogenic' tryptophan residues in calcium-binding EGF domains of short fibulin proteins. Experimental Eye Research, 130, 66–72. 10.1016/j.exer.2014.12.002 [PubMed: 25481286]

Popescu NI, Lupu C, & Lupu F. (2010). Extracellular protein disulfide isomerase regulates coagulation on endothelial cells through modulation of phosphatidylserine exposure. Blood, 116(6), 993–1001. 10.1182/blood-2009-10-249607 [PubMed: 20448108]

Ramadurgum P, & Hulleman JD (2020). Protocol for designing small-molecule-regulated destabilizing domains for in vitro use. STAR Protocols, 1, 100069. 10.1016/j.xpro.2020.100069

Ramadurgum P, Woodard DR, Daniel S, Peng H, Mallipeddi PL, Niederstrasser H, Mihelakis M, Chau VQ, Douglas PM, Posner BA, & Hulleman JD (2020). Simultaneous control of endogenous and user-defined genetic pathways using unique ecDHFR pharmacological chaperones. Cell Chemical Biology, 27(5):622–634.e626. 10.1016/j.chembiol.2020.03.006

Resnick E, Bradley A, Gan J, Douangamath A, Krojer T, Sethi R, Geurink PP, Aimon A, Amitai G, Bellini D, Bennett J, Fairhead M, Fedorov O, Gabizon R, Gan J, Guo J, Plotnikov A, Reznik N, Ruda GF, … London N. (2019). Rapid covalent-probe discovery by electrophile-fragment screening. Journal of the American Chemical Society, 141(22), 8951–8968. 10.1021/jacs.9b02822 [PubMed: 31060360]

Stone EM, Lotery AJ, Munier FL, Héon E, Piguet B, Guymer RH, Vandenburgh K, Cousin P, Nishimura D, Swiderski RE, Silvestri G, Mackey DA, Hageman GS, Bird AC, Sheffield VC, & Schorderet DF (1999). A single EFEMP1 mutation associated with both Malattia Leventinese and Doyne honeycomb retinal dystrophy. Nature Genetics, 22(2), 199–202. 10.1038/9722 [PubMed: 10369267]

Timpl R, Sasaki T, Kostka G, & Chu ML (2003). Fibulins: A versatile family of extracellular matrix proteins. Nature Reviews Molecular Cell Biology, 4(6), 479–489. 10.1038/nrm1130 [PubMed: 12778127]

Verlee M, Beyens A, Gezdirici A, Gulec EY, Pottie L, De Feyter S, Vanhooydonck M, Tapaneeyaphan P, Symoens S, & Callewaert B. (2021). Loss-of-function variants in EFEMP1 cause a recognizable connective tissue disorder characterized by cutis laxa and multiple herniations. Genes (Basel), 12(4):510. 10.3390/genes12040510 [PubMed: 33807164]

Woodard DR, Nakahara E, & Hulleman JD (2021). Clinically-identified C-terminal mutations in fibulin-3 are prone to misfolding and destabilization. Scientific Reports, 11(1):2998. 10.1038/s41598-020-79570-x [PubMed: 33542268]

Woodard DR, Xing C, Ganne P, Liang H, Mahindrakar A, Sankurathri C, & Mootha VV (2021). A novel homozygous missense mutation p.P388S in TULP1 causes protein instability and retinitis pigmentosa. Molecular Vision, 27, 179–190. [PubMed: 33907372]

Xiong W, Meisinger T, Knispel R, Worth JM, & Baxter BT (2012). MMP-2 regulates Erk1/2 phosphorylation and aortic dilatation in Marfan syndrome. Circulation Research, 110(12), e92–e101. 10.1161/CIRCRESAHA.112.268268 [PubMed: 22550139]

Zhang Y, & Marmorstein LY (2010). Focus on molecules: fibulin-3 (EFEMP1). Experimental Eye Research, 90(3), 374–375. [PubMed: 19799900]

Zimmermann DR, Trueb B, Winterhalter KH, Witmer R, & Fischer RW (1986). Type VI collagen is a major component of the human cornea. FEBS Letters, 197(1-2), 55–58. 10.1016/0014-5793(86)80297-6 [PubMed: 3512309]

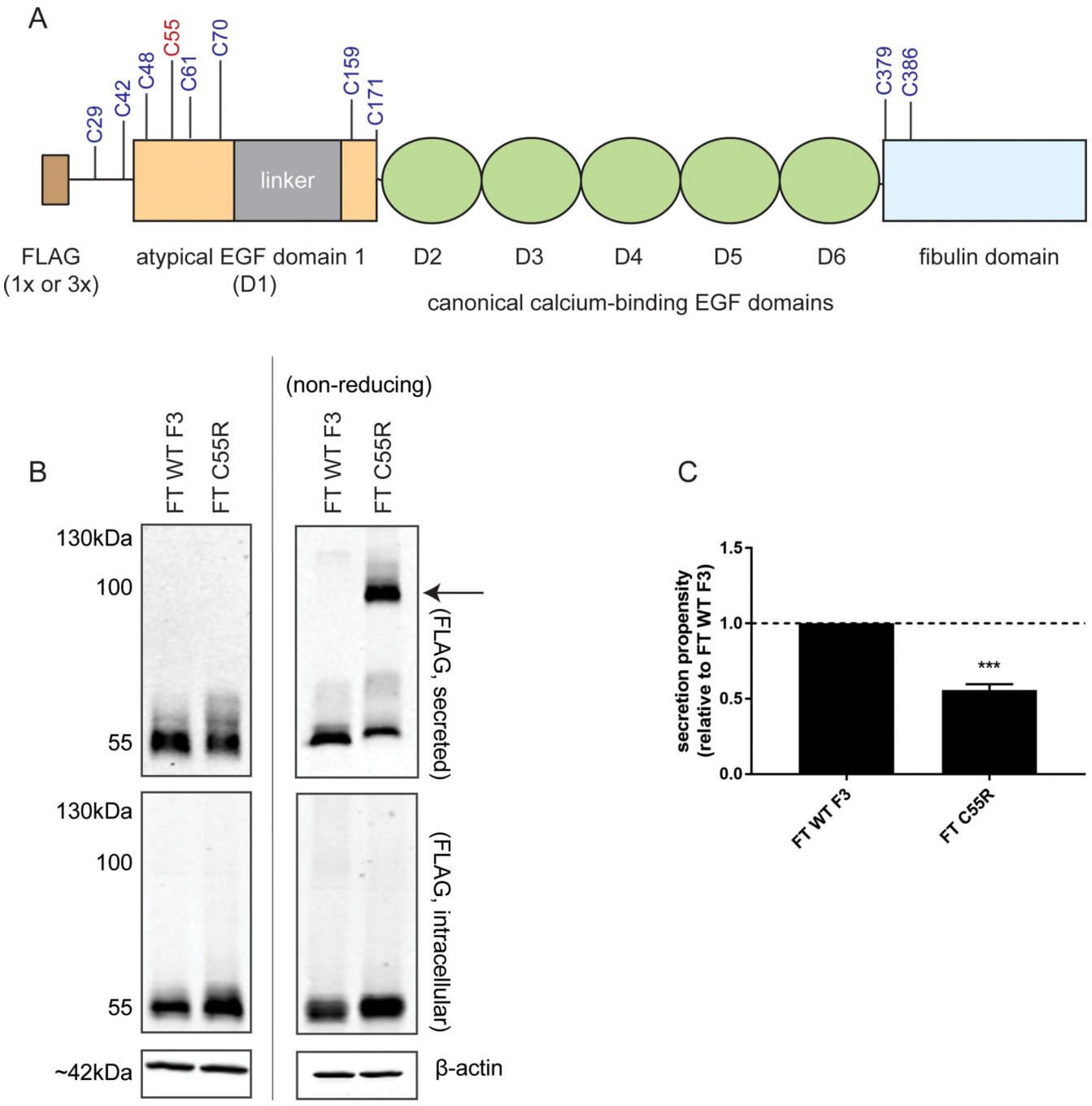

FIGURE 1.

The p.C55R mutation in F3 results in extracellular disulfide-linked dimerization. (a) Cartoon schematic of F3 by highlighting 10 cysteines that are either in a free confirmation or are not annotated in the Uniprot database (Q12805). The pathogenic p.C55R mutation associated with marfanoid syndrome is highlighted in red. (b) Western blot of secreted and intracellular FLAG-tagged (FT) WT F3 and p.C55R variants from transfected HEK-293A cells under reducing (left) or nonreducing (right) conditions. Arrow indicates p.C55R dimerization. (c) Quantitation of p.C55R secretion propensity compared to WT F3. $n = 7$, mean ±

standard error of the mean (***$p < 0.001$, one sample t-test vs. hypothetical value of 1 [i.e., unchanged]).

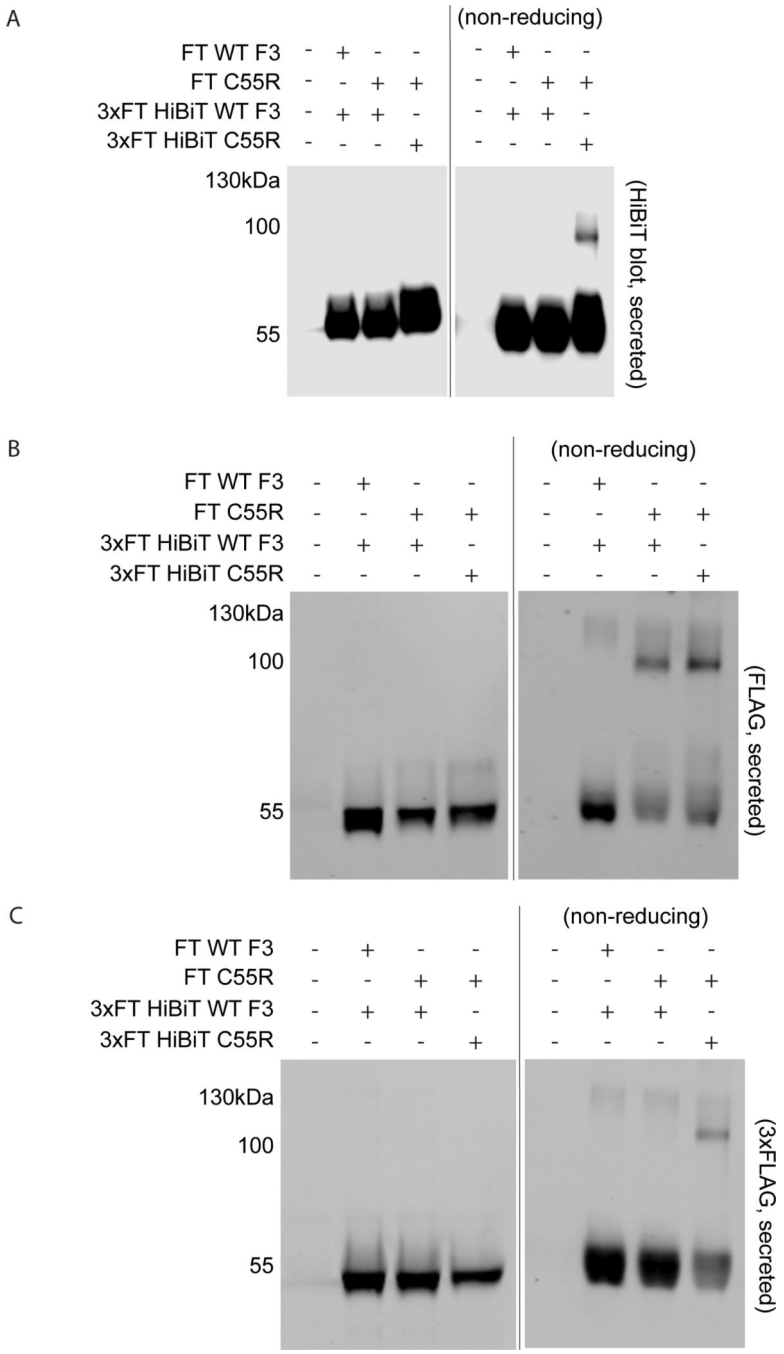

FIGURE 2.

p.C55R forms a disulfide-linked homodimer and does not appear to sequester WT F3. (a–c) HEK-293A cells were cotransfected with constructs encoding for FT WT F3, FT p.C55R, 3xFT HiBiT WT F3, or 3xFT HiBiT p.C55R. After transfection, media was changed to serum-free and 24 h later the conditioned media was collected western blotting for (a) HiBiT (using LgBiT and NanoGlo substrate), (b) 1xFLAG (rabbit anti-FLAG; Thermo Fisher Scientific), or (c) 3xFLAG (mouse anti-FLAG M2; Sigma). Representative data of $n = 3$ independent experiments.

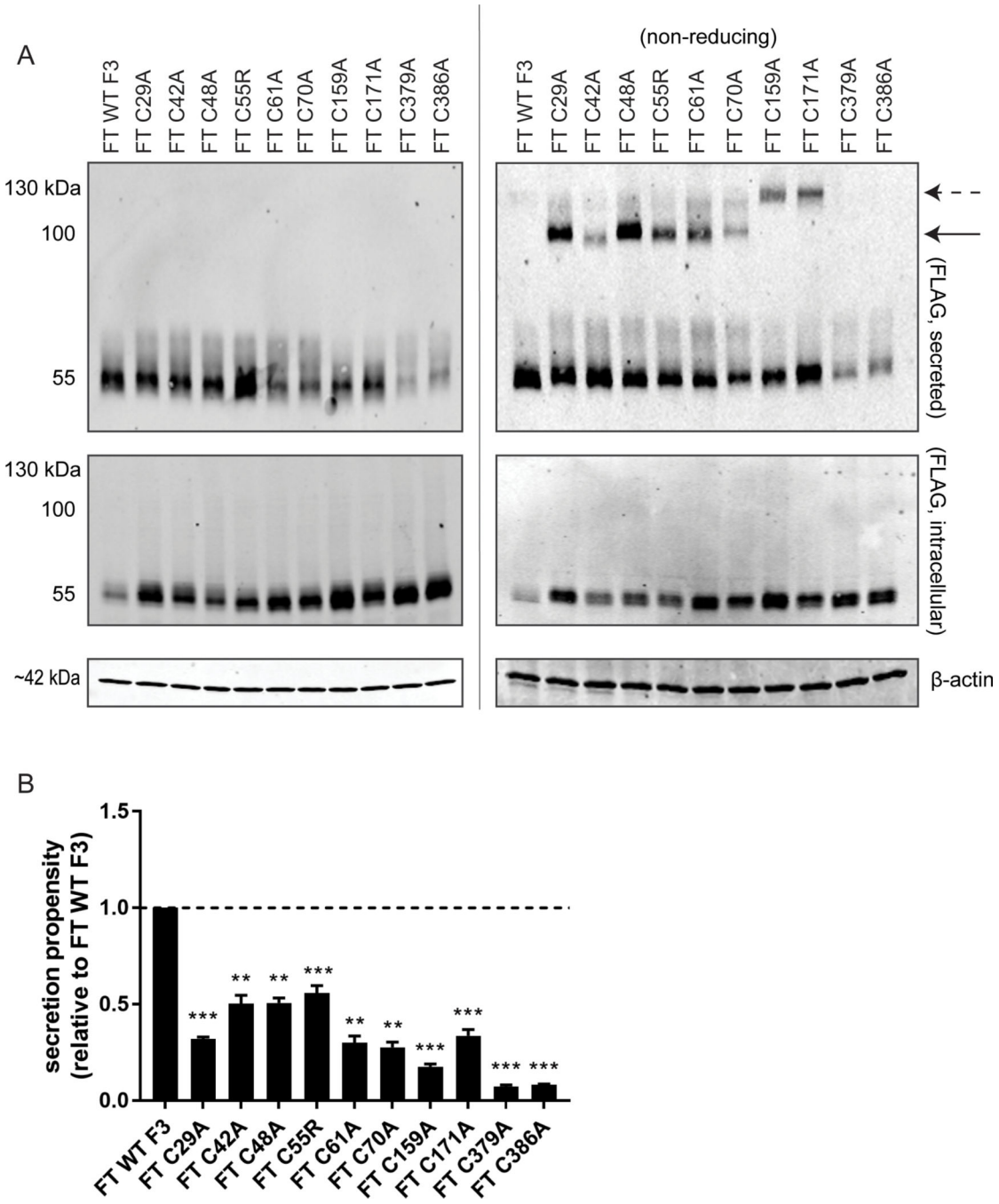

FIGURE 3.

Additional cysteine mutations in F3 lead to extracellular disulfide dimer formation. (a) Western blot of cysteine variants under reducing (left panel) and nonreducing (right panel) conditions. The solid arrow indicates the 110 kDa species while the dashed arrow represents an apparent 130 kDa species. (b) Quantification of secretion propensities in (a) (reducing conditions western was quantified), $n \geq 3$ independent experiments, mean ± standard error of the mean (**$p < 0.01$, ***$p < 0.001$, one sample *t*-test vs. hypothetical value of 1 [i.e., unchanged]).

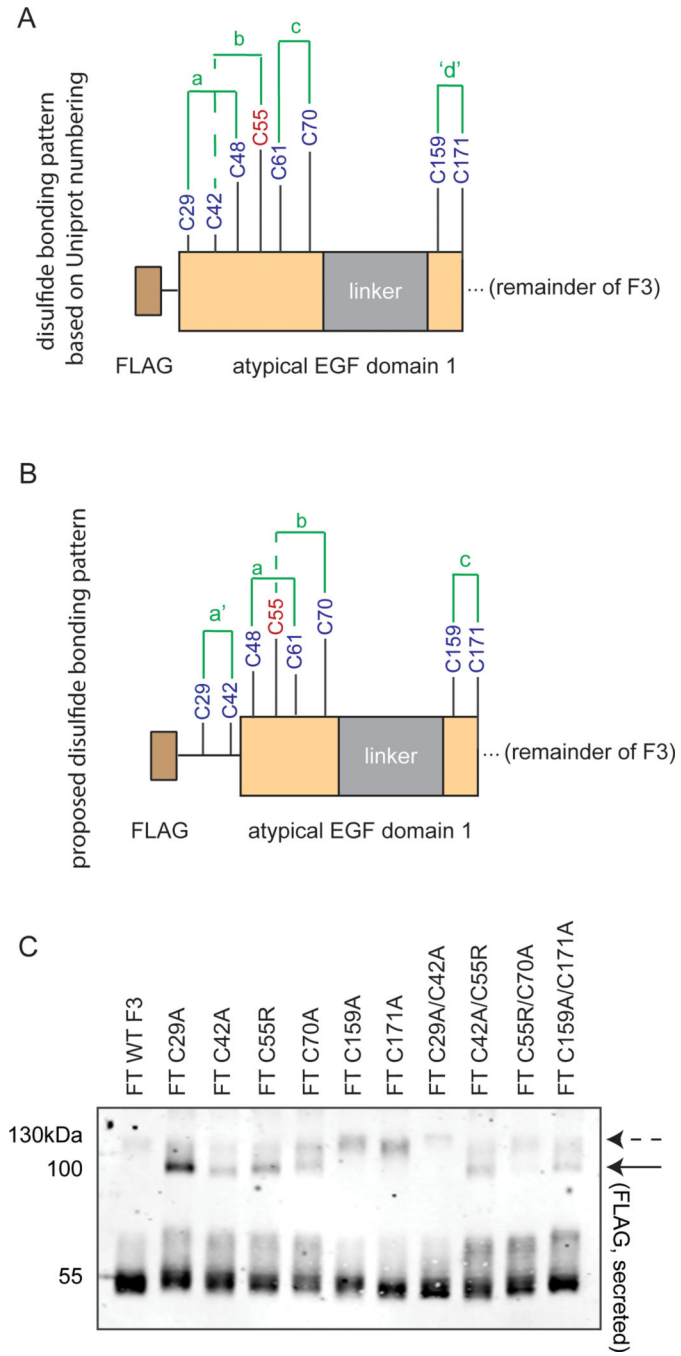

FIGURE 4.

Double cysteine mutations clarify disulfide bonding patterns in the atypical EGF domain of F3. (a) The predicted disulfide bonding pattern based on where Uniprot designates the start of the atypical EGF domain (at residue 26). (b) Proposed disulfide bonding pattern based on observations that all other F3 EGF domains begin with the amino acid sequence DIDE or DINE, which makes residue 44 the beginning of this domain. (c) Nonreducing western blotting for FT F3 was performed conditioned media from transfected HEK-293A cells. The

solid arrow indicates the 110 kDa species while the dashed arrow represents an apparent 130 kDa species. $n = 4$ independent experiments.

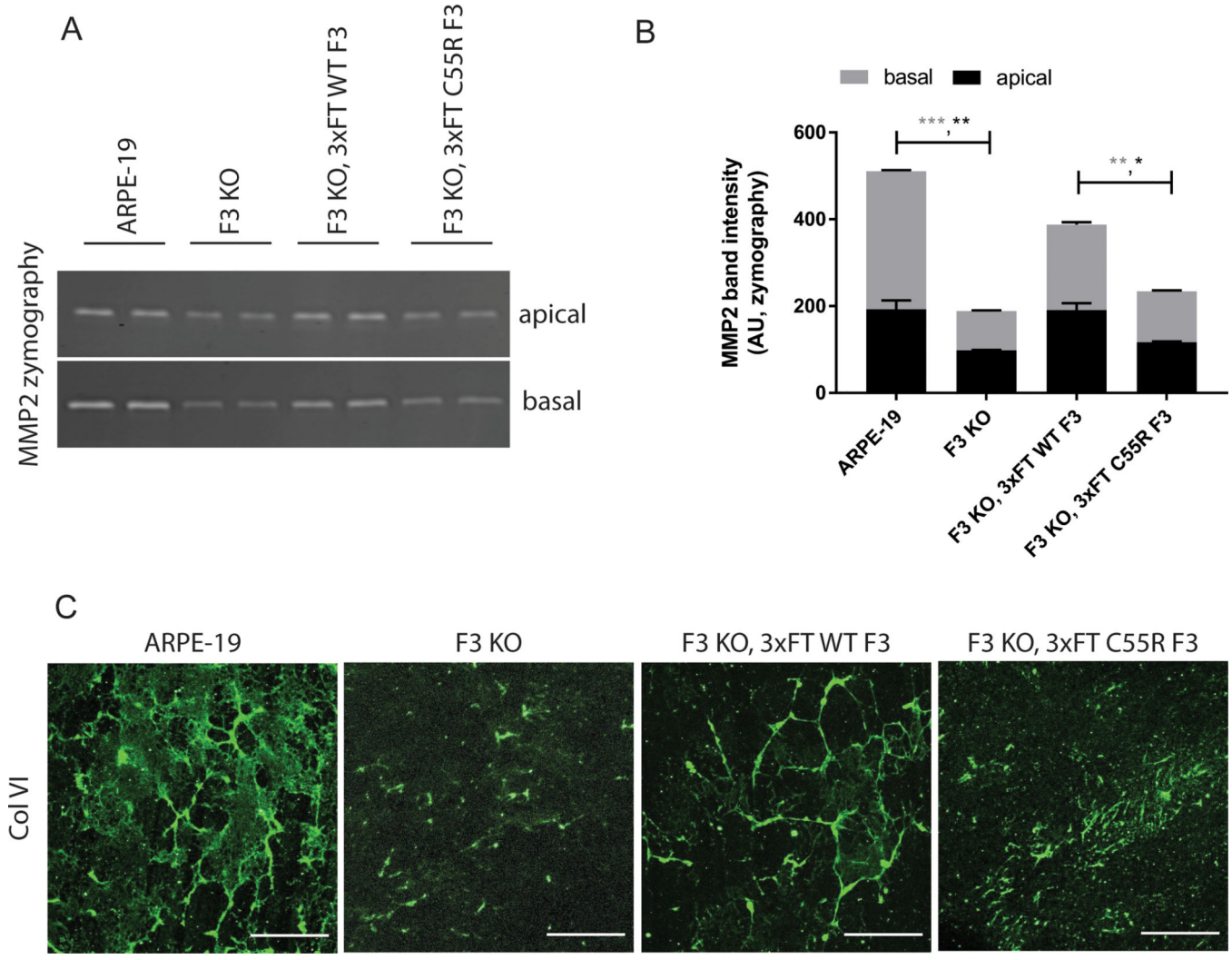

FIGURE 5.

Expression of p.C55R F3 is unable to compensate for loss of F3, leading to changes in ECM proteins and enzymes. (a) MMP2 zymography was performed on conditioned media samples from the indicated cell lines which were polarized on transwells for 2 weeks. (b) Quantification of absolute band intensity of gels shown in (a). Experiments were performed using at least biological duplicates and was performed ≥3 independent times. *$p < 0.05$, **$p < 0.01$, and ***$p < 0.001$, two-sample unpaired t-test. (c) ColVI ECM analysis from the indicated engineered cell lines polarized on transwell inserts for 2 weeks. Transwell membranes were decellularized, fixed, stained, and imaged using confocal microscopy. Representative data of $n = 2–3$ independent experiments, scale bar = 50 μm.